Author Contributions:

Conceptualization: Wei Li, Junhui Wang, Zhiyuan Ge, Xingguo Huang
Formal analysis: Zhiyuan Ge, Xingguo Huang
Funding acquisition: Zhiyuan Ge
Investigation: Wei Li, Junhui Wang, Xingguo Huang
Methodology: Junhui Wang
Project administration: Junhui Wang, Xingguo Huang
Software: Wei Li
Supervision: Junhui Wang, Zhiyuan Ge, Xingguo Huang
Visualization: Wei Li
Writing – original draft: Wei Li

The Topset-Foreset Rollover Does Not Coincide With Real Shoreline Positions in Clinoforms Over Substrate Deformation

Wei Li[1,2] ⓘ, **Junhui Wang**[1,2] ⓘ, **Zhiyuan Ge**[1,2] ⓘ, and **Xingguo Huang**[3] ⓘ

[1]State Key Laboratory of Petroleum Resources and Engineering, China University of Petroleum (Beijing), Beijing, China, [2]College of Geosciences, China University of Petroleum (Beijing), Beijing, China, [3]College of Instrumentation and Electrical Engineering, Jilin University, Changchun, China

Abstract Shoreline trajectories are migration path lines of topset-foreset rollovers in clinoforms. Stratigraphic trajectory analysis is largely based on its reflection of historical shoreline positions. However, this assumption is valid only when the substrate remains stable. In this study, we conducted numerical simulations and quantitative analyses to investigate the impact of gravity-driven deformation on shoreline trajectories. In a simulation with a rigid substrate, the shoreline trajectory initially moved basinward and then retreated landward, following the theoretical autoretreat in response to steady relative sea level (RSL) rise. In a simulation with a viscous substrate, the occurrence of syn-depositional deformation resulted in a much more complex shoreline trajectory, even with the same sediment supply and sea level rise. Our findings explicitly demonstrate that shoreline trajectory is not only controlled by the sediment supply and RSL change but also substrate deformation. Identifying syn-depositional deformation is critical in reconstructing shoreline evolution and avoiding misinterpretation.

Plain Language Summary Identifying the migration paths of shorelines within deltaic systems is a well-known method for reconstructing ancient sea levels and gaining insights into basinal stratigraphy. A key step in the analysis of shoreline trajectories is using the ancient shoreline trajectory to reconstruct the shoreline positions during basin evolution. However, if the substrate beneath the delta deforms during the evolution of the depositional system, the shoreline trajectories may not accurately represent the actual shoreline migration process. Here, we explore how changes in shoreline trajectories are affected by a viscous underlying layer. We find that deformation of the viscous layer disrupts the morphology of the overlying strata and alters the migration trajectory of the shoreline. Therefore, this study bears important implications for interpreting and analyzing ancient sea level change in tectonically active regions.

1. Introduction

The shoreline trajectory is the trajectory of the topset-foreset slope break within basin marginal strata sections and is an important concept of genetic stratigraphic interpretation (Catuneanu et al., 2009; Helland-Hansen & Gjelberg, 1994; Helland-Hansen & Martinsen, 1996; Henriksen et al., 2009; Mellere et al., 2002) (Figure 1a). The analysis of shoreline trajectory relies on the assumption that such breaks indicate ancient shoreline positions so that we can use this as a proxy for RSL evolution. The analysis is the cornerstone of the theory to explain how strata are stacked in response to RSL change and predicts the associated lithological distribution (Helland-Hansen & Martinsen, 1996; Jia et al., 2021; Vail et al., 1977).

For the above assumption to be effective, a necessary condition is that the substrate must be static so that it does not modify the general geometry of the overlying strata, by which the topset-foreset rollover correctly records the ancient shoreline position (Patruno et al., 2015; Patruno & Helland-Hansen, 2018; Pirmez et al., 1998; Steel et al., 2008; R. Steel & Olsen, 2002). In tectonically active basins, however, post-depositional and syn-depositional deformation may fundamentally change the rollover geometry thus distorting the real trajectory migration. For example, some studies have noted that gravity-driven systems (i.e., gravity spreading and gravity gliding) with an underlying viscous layer can alter the clinoform morphology (Cohen & Hardy, 1996; Ge et al., 1997; Minelli et al., 2013; Mourgues et al., 2009; Rojo et al., 2020), leading to the cross-directional displacement of the stacking strata. In these cases, existing shoreline trajectories and real shoreline evolution

Writing – review & editing: Wei Li, Junhui Wang, Zhiyuan Ge, Xingguo Huang
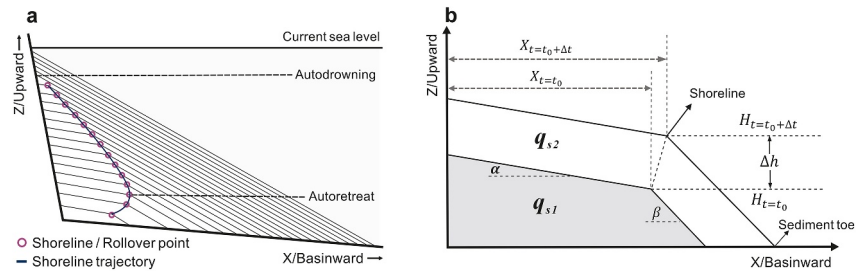
Figure 1. Illustration showing the shoreline trajectory and shoreline autoretreat. (a) Shoreline trajectory and the process of autoretreat. Different periods of rollover point connect sequentially to form a shoreline trajectory, which can be used to analyze the timing of autoretreat and autodrowning. (b) The sediment distribution pattern of shoreline autoretreat model. The intersection of the topset and the foreset indicates the shoreline position. α is topset slope, β is foreset slope, R_{bl} is relative sea level rise rate, Δt indicates a particular time interval, and q_{s_1} and q_{s_2} are sediment supply during Δt (i.e., $q_{s_1} = q_{s_2} = q_s \times \Delta t$) (Adapted from Wang et al., 2020, 2024).

do not coincide. However, how such deformation modifies shoreline positions and trajectories through time and space and what the main controls remain unclear.

Here, we aim to study the influence of viscous substrate on the overlying shoreline position by using the autoretreat deltaic systems as an example. With the numerical finite element method, we simulate two deltas without and with viscous substrate during steady sea level rise, respectively. We then quantitatively analyze the impact of the viscous substrate before discussing how the viscous substrate results in a variation between the apparent shoreline trajectory and the real shoreline trajectory. This study thus provides a reference for using the apparent shoreline trajectory to reveal the evolution of clinoforms in tectonically active regions.

2. Methods

2.1. The Theory of Shoreline Autoretreat

We use the shoreline autoretreat model (Muto & Steel, 1992) as a base model (Figure 1a), which captures the shoreline trajectory in a constant sea level rise scenario (Kim et al., 2006). The theory of shoreline autoretreat predicts that for an alluvial-deltaic system growing with a steady RSL rise and a constant sediment supply, the shoreline initially advances basinward and then inevitably retreats landward in an overall upward trend (Muto & Steel, 1992). The shoreline trajectory of any such system is deterministic with given rates of sea level rise (R_{bl}) and sediment supply (q_s), as well as slope parameters including the hinterland slope (γ), the basin floor slope (ϕ), the topset slope (α) and the foreset slope (β) (Figure 1b). In a two-dimensional X-Z coordinate system (the intersection point of the hinterland basement and the basin floor is set as the original point, where X is positive basinward and Z is positive upward) relative to the initial position of the shoreline (0, 0), when the forcing is steady (i.e., R_{bl} = constant > 0, q_s = constant > 0), the shoreline trajectory of the autoretreat delta can be predicted using the following equations:

$$x = (\tan \phi)^{-1} \times \left(-y + \sqrt{czD}\right) \tag{1}$$

$$c = 2(\tan \beta - \tan \alpha) \times \frac{\tan \phi - \tan \alpha}{\tan \beta} \times \left(1 - \frac{\tan \alpha}{\tan \beta}\right)^{-1} \tag{2}$$

where $D = \frac{q_s}{R_{bl}}$ control the potential growth rate of the delta, z is the height attained of shoreline and its equivalent to the product of R_{bl} and the time elapsed. Therefore, Equation 1 also describes the relationship between the migration of the shoreline (x) and time (t) (Muto, 2001).

This study integrates previous research and natural cases to deploy a set of typical parameters for the autoretreat model. The rate of sea level rise is typically less than 10 mm/yr (Kopp et al., 2009), we adopted a conservative value of R_{bl} = 2.2 mm/yr. In our model, sea level is treated as an independent variable, unaffected by either tectonic deformation or sediment input (Rovere et al., 2016). We estimate the sediment supply as q_s = 3.6 m^2/yr using aggradation and progradation rates reported in previous studies, which typically fall within the values
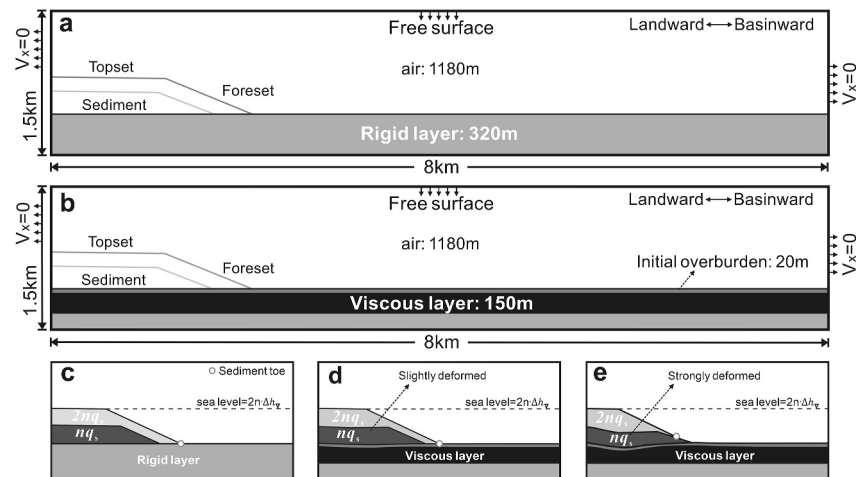
Figure 2. Illustration of the numerical model setup. (a) Model 1 has a rigid substrate layer. (b) Model 2 has a viscous substrate layer. The boundary velocity of both models is zero, indicating that there are no external extensional or contractional tectonic forces. Note the initial condition of the viscous salt is horizontal and has a uniform thickness. (c) Sketch showing the sediment filling pattern without a viscous layer, as in Figure 1b. (d, e) Illustration of sediment filling pattern of Model 2. As gravity-driven deformation starts with sediment loading, the topsets deform and eventually trap most of the sediments. Thus, the position of the sediment toe progrades forward and retreats backward when the deformation is mild and strong, respectively. The position of the sediment toe, effectively depends on the degree of deformation of the overlying strata (and substrate).

between 0.1 and 10 m^2/yr (Chamberlain et al., 2018; Jenkins, 2018; Ritchie et al., 2004; J. Wang & Muto, 2021). The topset angle is small, while the foreset angle largely depends on the sediment composition and is typically less than 30° (Patruno & Helland-Hansen, 2018; Prather et al., 2017). The selection of high-angle slopes ($\alpha = 1°$ and $\beta = 15°$) contributes to the occurrence of autoretreat and triggers gravitational instability (Swenson et al., 2000; Vendeville, 2005).

2.2. Numerical Modeling

To simulate the process of substrate deformation, we utilized a finite element numerical approach, which has been successfully tested for studying the dynamic interaction between sediments and salt flow (Albertz & Ings, 2012; Goteti et al., 2012; Hamdani et al., 2021; Ings & Beaumont, 2010; Pichel et al., 2024). In this study, the finite element method is based on Underworld2 (Beucher et al., 2019; Mansour et al., 2020). The modeling foundations of geodynamics and the mathematical theory of the Underworld can be found in Moresi et al. (2003, 2007). We conducted a series of models (Models Sr1-Sr2 and Models Sv1-Sv5, in supporting Information S1) to test the relative importance of various parameters (e.g., sedimentation rate, salt thickness, salt viscosity, and basement tilting) before constructing two two-dimensional models (Models 1 and 2) with and without a viscous substrate layer. The two models using the same input parameters (Table S1 in supporting Information S1), physical scales, and simulation times. In Model 1, the delta undergoes autoretreat on a static substrate without deformation. In Model 2, the substrate is viscous which is modeled by salt of 150 m thickness (h_{salt}).

Both finite element models are set 8 km in length and 1.5 km in height and consist of 800 and 200 regular meshes, respectively. For Model 1, the material composition is a 1,180 m air layer, and a 320 m rigid layer for deltaic sedimentation (Figure 2a). Model 2 contains a 1,180 m air layer, a 20 m initial overburden (Brun & Fort, 2011), a 150 m salt layer, and an undeformed basement (Figure 2b). The gray line used to represent topset and foreset in Figures 2a and 2b indicates the location of the supplied sediment as it progresses from landward to basinward. Note that the different sediment filling pattern between Model 1 (Figure 2c) and Model 2 (Figures 2d and 2e) is due to accommodation variation in the proximal part of the model. The deformation of the model is solely driven by sediment overburden added during the numerical simulation (Table S2 in supporting Information S1).

As sea level rose for 400 kyr (Figure 3), both models generated two kinds of shoreline trajectories, namely the real and apparent ones (Figure 4). For the real shoreline position, we recorded the real-time shoreline position of the delta every 10,000 years during model evolution. These recorded positions were then connected chronologically
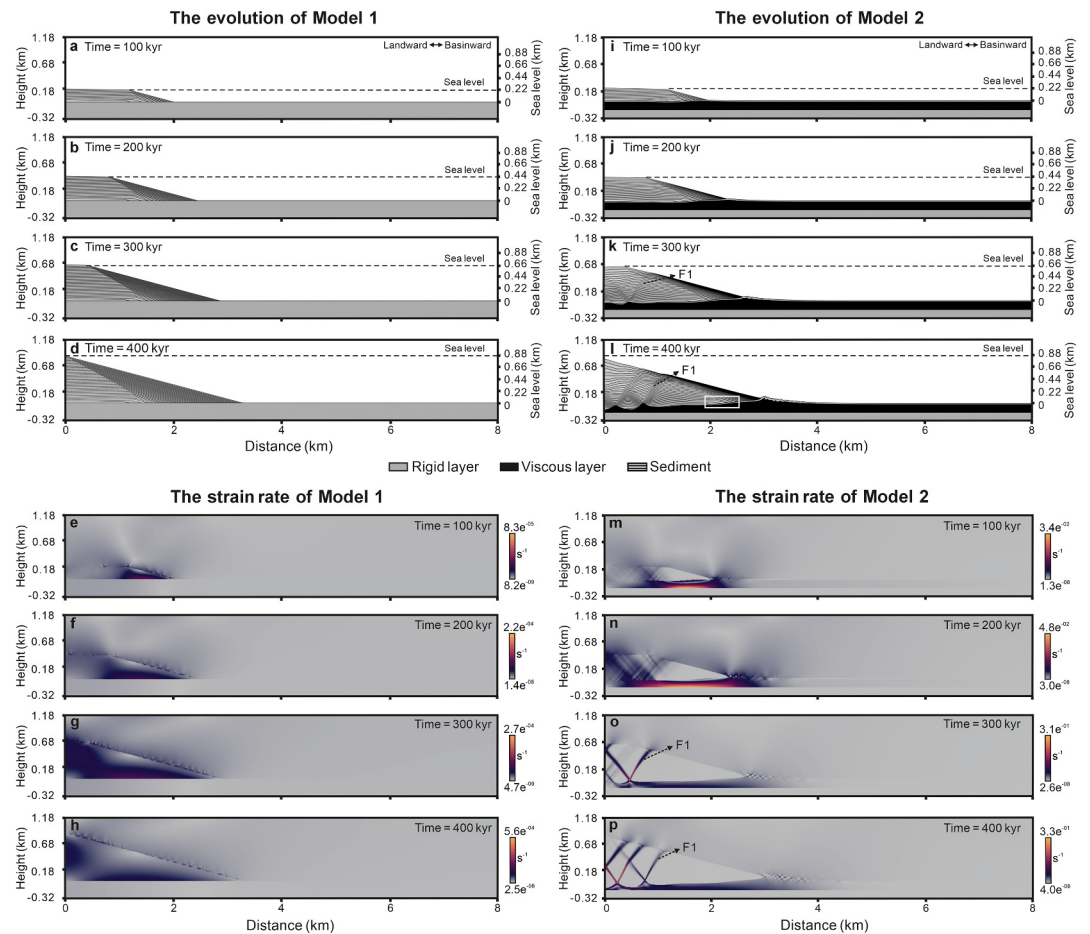
Figure 3. Stratigraphic configuration and strain rate in Model 1 and Model 2 at selected times. (a–d) Modeling results of Model 1 showing the process of shoreline autoretreat at 100, 200, 300, and 400 kyr. During the process of shoreline retreat, the topset became narrower and eventually was submerged as the foreset became longer and the buried shoreline trajectory remained unchanged. (e–h) Strain rate of the Model 1 corresponding stratigraphic configurations of a–d. The rigid substrate was not deformed and no faults developed on the slope. (i–l) Modeling results of Model 2 at 100, 200, 300, and 400 kyr. In the early stages (i, j), the deformation of the underlying viscous layer was mild and shoreline autoretreat took place. From (k) to (l), as more sediments accumulated to drive deformation, the viscous substrate flowed faster toward the basin. As a result, the overlying strata were deformed and the foreset toe was pushed basinward. (m–p) Strain rate of the Model 2 corresponding to i–l. The deformation in the viscous layer was intense and faults grew over the delta slope. Note the strain rates in Model 2 are 2–3 orders of magnitude higher than that in Model 1.

showing the real shoreline trajectory (Figures 4a and 4b). After the simulation, following the traditional clinoform analysis, we identified slope breaks from the final evolutionary profiles of the two models (Figures 4a and 4b), which we referred to as apparent shoreline trajectories. We also recorded the movement trajectory of the first shoreline position through time in Model 2 (Figure 4b).

We use Root Mean Square Error (RMSE) and Mean Absolute Percentage Error (MAPE) to assess the degree of discrepancy between different trajectories (the closer to 0, the smaller the difference). In addition, we use Pearson correlation coefficient (PCC) and Spearman correlation coefficient (SCC) to evaluate the similarity of the changing trends between different trajectories (the closer to 1, the higher the similarity) (Das et al., 2023).

3. Results

3.1. Pilot Models and Sensitivity Tests

We conducted seven pilot models to show that salt thickness and viscosity are the most important parameters for the overlying strata to deform (Figures S1–S6 in supporting Information S1). Specifically, thicker (≥150 m) and
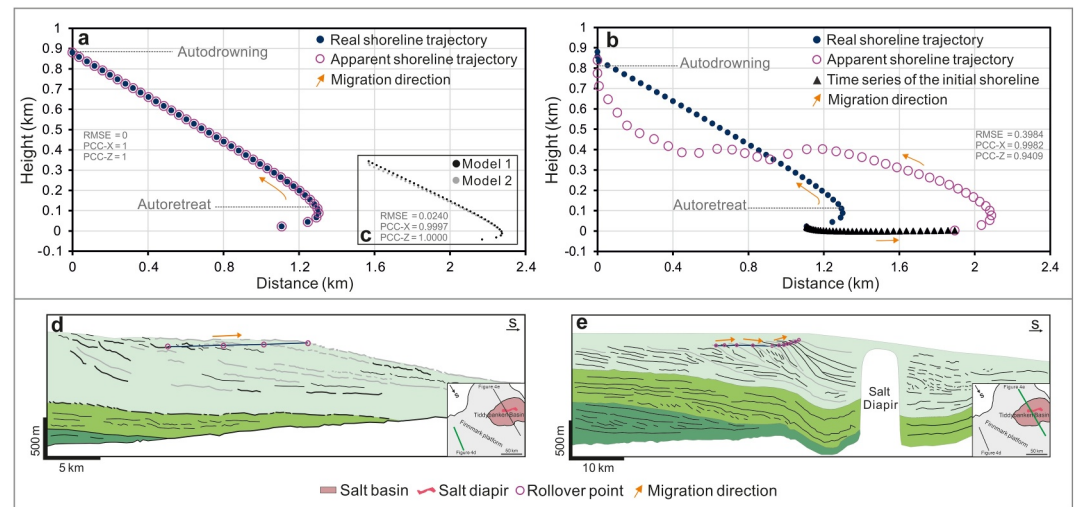
Figure 4. The real and apparent shoreline trajectories for the two models and two natural examples. (a) Model 1, with the stable substrate, the real shoreline trajectory and the apparent shoreline trajectory are identical. (b) Model 2, significant discrepancies exist between the real and apparent shoreline trajectories. The triangle indicates the historical positions of the first shoreline position, which moved from $X = 1.11$ km at the beginning to $X = 1.89$ km at the end of the simulation. (c) Comparison of the real shoreline trajectory between Model 1 and Model 2. (d) and (e) are the interpreted seismic sections, located in the Norwegian Barents Sea. (d) The clinoforms without an active viscous substrate, and the rollover point exhibits a single raised trajectory. (e) The clinoforms develop over the salt layer, where the migration direction of the rollover curve has changed several times (Adapted from Rojo et al., 2020).

less viscous ($\leq 10^{18}$ Pa · s) salt can facilitate the syn-depositional deformation and influence the modification of the autoretreat system. Other parameters, such as basement tilting, only have secondary controls on model behaviors, with minor variations observed between the real and apparent shoreline trajectories in the associated models (Models Sv1 and Sv4).

3.2. Model 1: Rigid Substrate

In Model 1, the process of shoreline autoretreat was successfully modeled. During the first 40 kyr of 400 kyr simulation time, the shoreline advances basinward. From 50 kyr onward, the shoreline retreated landward while aggrading for the next 350 kyr until the topset was totally submerged at 400 kyr (Figures 3a–3d). In addition, there was no deformation or fault growth on the overlying strata and static substrate (Figures 3e–3h), as the substrate was stable so that the geometry of the overlying strata remained undeformed during the whole simulation. Therefore, the final position of topset-foreset rollover records the historical shoreline positions, suggesting that the real and the apparent shoreline trajectories are identical (Figure 4a).

3.3. Model 2: Viscous Substrate

In Model 2, unlike the real shoreline trajectory, the apparent shoreline trajectory had been strongly modified by gravity-driven deformation (Figures 3i–3l). The overburden began to deform soon after sediment deposition as faults nucleated and grew within the sediment wedge (Figures 3m–3p). This is revealed by the continuous seaward movement of the first shoreline position (Figure 4b). From 50 kyr, the real shoreline trajectory exhibited an accretionary transgressive pattern, and continued until 390 kyr when the topset was submerged. During the process, until 220 kyr, the apparent shoreline trajectory showed a similar trend as the real shoreline from ascending regression to accretionary transgression, because the shoreline was on the tilted frontal slope of the sediment wedge where no fault occurred (Figures 3i and 3j). However, the tilted depositional slope pushed the apparent shoreline trajectory slightly downward compared with the real one due to the basinward extension and depletion of viscous salt underneath (Figure 3j). From 230 kyr onwards, as the real shoreline retreated to the extensional domain of the sediment wedge, the normal fault F1 started to modify the apparent shoreline trajectory by forcing it to transgress accretionary (Figure 3k). This modification only stopped at 310 kyr when the real shoreline position moved away from the fault-influenced region (Figure 3l), and the apparent shoreline started to

transgress accretionary again (Figure 4b). However, the apparent shoreline trajectory continued to be lower than the real one due to continuous salt depletion underneath (Figure 4b). After 300 kyr, upstream sediment supply to the delta toe ceased (Figures 3k and 3l), leading to topset drowning at 390 kyr (e.g., Figure 2f).

4. Similarity Analysis Between the Real and Apparent Shorelines

The trajectory variations can be further validated using quantitative metrics. For Model 1, RMSE and MAPE of the apparent shoreline trajectory relative to the real shoreline trajectory are 0% and 0%, respectively (Table S4 in supporting Information S1), and PCC and SCC values are both one in the X and Z directions, indicating that the two curves are identical. For Model 2, RMSE and MAPE of the apparent shoreline trajectory relative to the real shoreline trajectory are 0.3984 km and 38.26%, respectively (Table S4 in supporting Information S1), indicating strong modification of shoreline positions by the viscous substrate. Moreover, although the two trajectories exhibit very similar changing trends, the PCC values in the X and Z directions are 0.9982 and 0.9409, while the SCC values are 0.9994 and 0.9750 (Table S5 in supporting Information S1). These values suggest the salt layer exerts a more pronounced influence in the vertical direction (Figure S8 in supporting Information S1), as both PCC and SCC values are smaller in the Z direction. This effect is primarily due to shoreline modifications induced by the normal fault F1 in the model.

In addition, we analyzed the real shoreline trajectories in the two models. RMSE and MAPE of Model 2 relative to Model 1 are 0.0241% and 6.01%, respectively (Table S4 in supporting Information S1). PCC values in the X and Z directions are 0.9997 and 1.0000, while SCC values are 0.9999 and 1.0000 (Table S5 in supporting Information S1). These values suggest that the two real shoreline trajectories maintain close spatial proximity and strong correlation, yet are different in essence due to the syn-depositional deformation involved in Model 2.

5. Discussion

5.1. Difference Between the Real and Apparent Shoreline Trajectories

Previous studies focusing on tectonically active basins have recognized that structural evolution has a direct impact on stratigraphic stacking patterns (Hampson et al., 2009; Patruno & Helland-Hansen, 2018; Rojo et al., 2020; R. Steel & Olsen, 2002). Our study confirms that the syn-depositional deformation can modify the rollover geometry of the apparent shoreline (Figure S7 in supporting Information S1), but has limited impact on the real shoreline trajectory. In Models 1 and 2, both real shoreline trajectories have very similar lengths and trends that characterize a typical autoretreat pattern, indicating that the gravity-driven deformation has little influence on the real shoreline trajectory. In contrast, the syn-depositional deformation alters the apparent shoreline position, as recorded by the time series curve of the first shoreline position in Model 2 (triangle in Figure 4b). Notably, the apparent shoreline trajectory retreated downward from 230 to 310 kyr, when the shoreline migrated over the normal fault F1 and moved along with its subsiding hanging wall, reversing the upward trend of the real shoreline positions observed in Model 2 (Figures 3k and 3o). This phenomenon is also supported by the quantitative analysis as the smaller values of the Pearson and Spearman correlation coefficients of the Z axis indicate more pronounced salt influences along the vertical direction (Figure S8 in supporting Information S1).

The deformation occurred in Model 2 is thin-skinned and gravity-driven, controlled by differential sediment loading of the delta (Cobbold & Szatmari, 1991; Fort et al., 2004; Rowan et al., 2004). Specifically, as the sediment accumulates over the viscous layer, the inclined topset and foreset (i.e., clinothem) generate a pressure head gradient, by which the viscous salt flows from high to low pressure regions (Fort et al., 2004; Rowan et al., 2004; Vendeville & Jackson, 1992). Such pressure distribution forms a linked deformation system of landward extension and basinward contraction with a transitional domain in between (Ge et al., 1997; Vendeville, 2005). The apparent shoreline maintained a similar retreating trend as the real one when it was in the transitional domain of the front slope, where no significant deformation was observed. When the shoreline retreated to the area of the extensional domain, the apparent shoreline trajectory was effectively controlled by the normal fault F1 (Figures 3k and 3l). Such strong modification of the apparent shoreline suggests a direct structural control on the stratigraphic evolution. This phenomenon is comparable to the stratigraphic stacking pattern observed in rifts where shoreline trajectories are dominated by faulting style and associated fault growth (Gawthorpe et al., 1994). However, the shoreline trajectory in our model is much more complex because the deltaic sedimentation and syn-depositional deformation are deeply coupled. The resulting variation between real

and apparent shoreline trajectories is governed by the feedback mechanism between sedimentation and gravity-driven deformation.

5.2. Influence of Syn-Depositional Deformation on Real Trajectory Reconstruction

The quantitative analysis reveals the presence of the viscous layer also leads to discrepancies in the real shoreline trajectories between Model 1 and Model 2, despite the overall similarity between the two curves (Figure 4c). Compared to Model 1, Model 2 developed an extension in its topset. allowing the stretching of the topset strata. In general, the effect of a longer topset benefits the occurrence of autoretreat as more sediments are trapped in the topset (Tomer et al., 2011). During the early stages of Model 2, the delta is inadequately scaled to instigate noticeable salt flows. Thus, the delta growth and shoreline migration are largely controlled by RSL change and sediment supply with limited structural disruption. Only after 230 kyr, when the accumulated extension was strong enough, the real shoreline trajectory of Model 2 was significantly lower than that of Model 1, which ultimately resulted in the early drowning of the topset. Interestingly, Model Sv3 of the sensitivity tests also shows that the thicker viscous layer allows the topset to drown even earlier, indicating a faster sediment subsidence and stronger salt flow (Figure S3 in supporting Information S1).

Tectonic induced topographic relief can fundamentally change the sediment partitioning within the sedimentary system, which has been amply demonstrated in extensional as well as contractional regions (Burbank et al., 1996; Jordan & Flemings, 1991; Liesa et al., 2006). The impact of such alternation has mixed influences on sediment stacking pattern in Model 2. On one hand, the syn-depositional deformation increased the ability of accommodating sediments in the topset, thus reduced the sediments propagating seaward. On the other hand, the subsidence rate of the topset exceeded its vertical growth rate and resulted in early drowning. This observation suggests that reconstructing the real shoreline or clinoform evolution can be very difficult, if not impossible, with syn-depositional deformation influencing contemporary deposition.

Another important corollary is that sediment accumulation can introduce isostatic subsidence and deformation because the lithosphere rests on a layer of low-viscosity and plastic asthenosphere (Conrad & Behn, 2010; Zhang et al., 2024). Our model only assumes a constant sediment supply rate for a typical deltaic clinoform which is a few tens of kilometers in length and up to a few hundred meters in thickness (Budai et al., 2021; Patruno & Helland-Hansen, 2018; Steel et al., 2024). Such depositional systems have a minor impact on isostatic balance due to the limited thickness. However, the isostatic force of another type of clinoform, the shelf-edge and continental margin clinoform, cannot be neglected, because such clinoforms usually extend across the margin with hundreds of kilometers in length and have sediment accumulated up to 10 km (Anell, 2024; R. Steel & Olsen, 2002). In a similar manner as our Model 2, the isostatic subsidence associated with shelf clinoforms can alternate the real clinoform trajectory. Unlike our simple system, natural sediment supply for such large sedimentary systems tends to vary significantly through space and time (Steckler et al., 1999; R. Steel & Olsen, 2002), which complicates base-level reconstruction quantification. Thus, trajectory analysis and base-level reconstruction for large-scale clinoforms may have some fundamental issues without considering isostatic balances.

5.3. Applications to Natural Systems

Traditional trajectory analysis provides a reliable reference for exploring RSL curves and associated clinoforms (Mikeš et al., 2015). In contrast, we cannot readily equate the apparent shoreline identified from the final profile of the trajectory to be the real shoreline if syn-depositional deformation exists. A notable example occurs in the Finnmark platform of the Barents Sea and its neighboring Tiddlybanken Basin (Gernigon et al., 2018; Paoletti et al., 2020; Rojo et al., 2020), where the former is not affected by salt-related deformation and the latter is a salt-bearing basin. Within the Finnmark platform, the rising basinward rollover trajectory shows a typical response to a continuous RSL rise (Figure 4d). In the Tiddlybanken Basin, the rollover trajectory migrated basinward during the same period, with a trend of going upward, downward, and upward again (Figure 4e). This variation in rollover trajectory has been interpreted as a result of local sea level variations associated with salt tectonic deformation, although the authors also suspected the clinoform trajectory might have been modified by salt tectonics after sediment deposition (Rojo et al., 2020). Given the Finnmark platform and its neighboring Tiddlybanken Basin are only 100 km apart and were both in a marine dominant environment from Aptian times (Heiberg, 2018), they tend to have the same RSL rise during the clinoform formation. Therefore, we suggest that the apparent rollover trajectory in the Tiddlybanken Basin is more likely to be primarily controlled by syn-

depositional deformation associated with salt tectonics rather than the local sea level changes. The slight downward movement of the rollover trajectory in the Tiddlybanken Basin can be interpreted as a part of the subsiding depocenter near the salt diapir (Figure 4e).

Observations from modern analogues also support the modification of rollover trajectory from deformation associated with an underlying viscous layer. For example, the Quaternary Acheloos delta in the Gulf of Patras, Greece has underlying Triassic evaporites and exhibits ongoing salt tectonic activity (Stathopoulou et al., 2025). The delta foreset displays upturned flaps flanking induced by salt diapir uplift, resulting in discrepancies between real and apparent shoreline trajectories, as suggested by our Model 2 (white box in Figure 3l).

The trajectory of topset-foreset rollover not solely reflecting shoreline history may be more common in nature than thought. Many other salt-bearing basins may also experience similar situations. For example, in the circum-Nile deformation belt or the Scotian Basin, the progradation of the clinoform sedimentary system drives the salt basinward (Albertz et al., 2010; Loncke et al., 2006), which can also hide the real shoreline trajectory. Moreover, many other kinds of substrate, such as shale and anhydrite, can facilitate gravity-driven deformation along basin margins (Cohen & Hardy, 1996; Dinc et al., 2022; Mourgues et al., 2009). Margin tilting associated with thermal subsidence also triggers gravity deformation (Ge et al., 2019; Karlo et al., 2014; Rowan et al., 2004). In addition, lithological variations inherent in basin margin strata can also induce differential compaction, leading to the reorientation of clinoform trajectories during syn-depositional deformation processes (Beelen et al., 2019). In these settings, distinguishing the real and apparent shoreline is important as they are vital to improving the accuracy of RSL interpretation and paleogeographic reconstructions. Although structural control is important, it does not change the significant effect of the interaction between sediment supply and RSL change on shoreline trajectories. For example, the wave-dominated deltas of the Fulmar Formation in the North Sea basin (Hampson et al., 2009), the shelf-edge delta of southern Wyoming (Carvajal & Steel, 2006), and the Rhône deltaic system of the NW Mediterranean (Berné et al., 2007) are all controlled by the imbalance between these two factors. Therefore, reconstructing real shoreline trajectory from sedimentary records needs to consider the combined influences from sea level change, sediment supply variation as well as syn-depositional deformation.

6. Conclusions

We use numerical models and quantitative analysis to investigate the effects of viscous substrate on shoreline trajectories and the mechanisms of gravity-driven deformation that lead to variations between the real and apparent shoreline trajectories. Our results show that when a viscous substrate is present, sedimentation can drive substrate movements and alter the post-depositional shoreline position thus conceal the real shoreline trajectory. This alteration not only results in the shoreline position recorded by the apparent rollover trajectory not being real but also constantly changes sediment dispersal thus also affecting the position of real shorelines. Therefore, both sedimentary system evolution and syn-depositional deformation exert fundamental controls on the geometry of shoreline trajectories. This study suggests that the variations between the apparent and real shorelines have important implications for stratigraphy analysis and RSL reconstruction, particularly in tectonically active regions.

Conflict of Interest

The authors declare no conflicts of interest relevant to this study.

Data Availability Statement

The code (Underworld) used in this study is available in http://www.underworldcode.org (Mansour et al., 2020). The shoreline position data from the models can be accessed at https://github.com/weilsalt/position-data.

References

Albertz, M., Beaumont, C., Shimeld, J. W., Ings, S. J., & Gradmann, S. (2010). An investigation of salt tectonic structural styles in the Scotian Basin, offshore Atlantic Canada: 1. Comparison of observations with geometrically simple numerical models. *Tectonics*, *29*(4), TC4017. https://doi.org/10.1029/2009TC002539

Albertz, M., & Ings, S. J. (2012). Some consequences of mechanical stratification in basin–scale numerical models of passive–margin salt tectonics. In G. I. Alsop, S. G. Archer, A. J. Hartley, N. T. Grant, & R. Hodgkinson (Eds.), *Salt Tectonics, Sediments and Prospectivity* (Vol. 363, pp. 303–330). Geological Society of London. https://doi.org/10.1144/SP363.14

Anell, I. (2024). The quintessential s-shape in sedimentology: A review on the formation and controls of clinoform shape. *Earth-Science Reviews*, *254*, 104821. https://doi.org/10.1016/j.earscirev.2024.104821

Beelen, D., Jackson, C. A.-L., Patruno, S., Hodgson, D. M., & Trabucho Alexandre, J. P. (2019). The effects of differential compaction on clinothem geometries and shelf-edge trajectories. *Geology*, *47*(11), 1011–1014. https://doi.org/10.1130/G46693.1

Berné, S., Jouet, G., Bassetti, M. A., Dennielou, B., & Taviani, M. (2007). Late Glacial to preboreal sea-level rise recorded by the Rhône deltaic system (NW Mediterranean). *Marine Geology*, *245*(1–4), 65–88. https://doi.org/10.1016/j.margeo.2007.07.006

Beucher, R., Moresi, L., Giordani, J., Mansour, J., Sandiford, D., Farrington, R., et al. (2019). UWGeodynamics: A teaching and research tool for numerical geodynamic modelling. *Journal of Open Source Software*, *4*(36), 1136. https://doi.org/10.21105/joss.01136

Brun, J.-P., & Fort, X. (2011). Salt tectonics at passive margins: Geology versus models. *Marine and Petroleum Geology*, *28*(6), 1123–1145. https://doi.org/10.1016/j.marpetgeo.2011.03.004

Budai, S., Colombera, L., & Mountney, N. P. (2021). Quantitative characterization of the sedimentary architecture of Gilbert-type deltas. *Sedimentary Geology*, *426*, 106022. https://doi.org/10.1016/j.sedgeo.2021.106022

Burbank, D., Meigs, A., & Brozović, N. (1996). Interactions of growing folds and coeval depositional systems. *Basin Research*, *8*(3), 199–223. https://doi.org/10.1046/j.1365-2117.1996.00181.x

Carvajal, R. C., & Steel, R. J. (2006). Thick turbidite successions from supply-dominated shelves during sea-level highstand. *Geology*, *34*(8), 665–668. https://doi.org/10.1130/G22505.1

Catuneanu, O., Abreu, V., Bhattacharya, J. P., Blum, M. D., Dalrymple, R. W., Eriksson, P. G., et al. (2009). Towards the standardization of sequence stratigraphy. *Earth-Science Reviews*, *92*(1), 1–33. https://doi.org/10.1016/j.earscirev.2008.10.003

Chamberlain, E. L., Törnqvist, T. E., Shen, Z., Mauz, B., & Wallinga, J. (2018). Anatomy of Mississippi Delta growth and its implications for coastal restoration. *Science Advances*, *4*(4), 4740. https://doi.org/10.1126/sciadv.aar4740

Cobbold, P. R., & Szatmari, P. (1991). Radial gravitational gliding on passive margins. *Tectonophysics*, *188*(3–4), 249–289. https://doi.org/10.1016/0040-1951(91)90459-6

Cohen, H. A., & Hardy, S. (1996). Numerical modelling of stratal architectures resulting from differential loading of a mobile substrate. *Geological Society, London, Special Publications*, *100*(1), 265–273. https://doi.org/10.1144/GSL.SP.1996.100.01.17

Conrad, C. P., & Behn, M. D. (2010). Constraints on lithosphere net rotation and asthenospheric viscosity from global mantle flow models and seismic anisotropy. *Geochemistry, Geophysics, Geosystems*, *11*(5), Q05W05. https://doi.org/10.1029/2009GC002970

Das, I., Morlighem, M., Barnes, J., Gudmundsson, G. H., Goldberg, D., & Dias dos Santos, T. (2023). In the quest of a parametric relation between ice sheet model inferred Weertman's sliding-law parameter and airborne radar-derived basal reflectivity underneath Thwaites Glacier, Antarctica. *Geophysical Research Letters*, *50*(10), e2022GL098910. https://doi.org/10.1029/2022GL098910

Dinc, G., Callot, J.-P., & Ringenbach, J.-C. (2022). Shale mobility: From salt-like shale flow to fluid mobilization in gravity-driven deformation, the late Albian–Turonian white pointer delta (Ceduna Subbasin, Great Bight, Australia). *Geology*, *51*(2), 174–178. https://doi.org/10.1130/G50611.1

Fort, X., Brun, J.-P., & Chauvel, F. (2004). Salt tectonics on the Angolan margin, synsedimentary deformation processes. *AAPG Bulletin*, *88*(11), 1523–1544. https://doi.org/10.1306/06010403012

Gawthorpe, R. L., Fraser, A. J., & Collier, R. E. L. (1994). Sequence stratigraphy in active extensional basins: Implications for the interpretation of ancient basin-fills. *Marine and Petroleum Geology*, *11*(6), 642–658. https://doi.org/10.1016/0264-8172(94)90021-3

Ge, H., Jackson, M. P. A., & Vendeville, B. C. (1997). Kinematics and dynamics of salt tectonics driven by progradation. *American Association of Petroleum Geologists Bulletin*, *81*, 398–423. https://doi.org/10.1306/522B4361-1727-11D7-8645000102C1865D

Ge, Z., Warsitzka, M., Rosenau, M., & Gawthorpe, R. L. (2019). The impact of instant versus progressive margin tilting upon passive margin salt basin structure. *Geology*, *47*(12), 1122–1126. https://doi.org/10.1130/G46485.1

Gernigon, L., Brönner, M., Dumais, M., Gradmann, S., Grønlie, A., Nasuti, A., & Roberts, D. (2018). Basement inheritance and salt structures in the SE Barents Sea: Insights from new potential field data. *Journal of Geodynamics*, *119*, 82–106. https://doi.org/10.1016/j.jog.2018.03.008

Goteti, R., Ings, S. J., & Beaumont, C. (2012). Development of salt minibasins initiated by sedimentary topographic relief. *Earth and Planetary Science Letters*, *339*, 103–116. https://doi.org/10.1016/j.epsl.2012.04.045

Hamdani, I., Aharonov, E., Olive, J.-A., Parez, S., & Gvirtzman, Z. (2021). Initiating salt tectonics by tilting: Viscous coupling between a tilted salt layer and overlying brittle sediment. *Journal of Geophysical Research: Solid Earth*, *126*(7), e2020JB021503. https://doi.org/10.1029/2020JB021503

Hampson, G., Sixsmith, P. J., Kieft, R. L., Jackson, C. A. L., & Johnson, H. D. (2009). Quantitative analysis of nettransgressive shoreline trajectories and stratigraphic arcitectures: Mid to late Jurassic of the North Sea basin. *Basin Research*, *21*(5), 528–558. https://doi.org/10.1111/j.1365-2117.2009.00414.x

Heiberg, V. (2018). *The regional Cretaceous development of the south-eastern part of the Norwegian Barents Sea - from seismic interpretation*. Master thesis. University of Tromsø.

Helland-Hansen, W., & Gjelberg, J. G. (1994). Conceptual basis and variability in sequence stratigraphy: A different perspective. *Sedimentary Geology*, *92*(1–2), 31–52. https://doi.org/10.1016/0037-0738(94)90053-1

Helland-Hansen, W., & Martinsen, O. J. (1996). Shoreline trajectories and sequences: Description of variable depositional-dip scenarios. *SEPM Journal of Sedimentary Research*, *66*(4), 670–688. https://doi.org/10.1306/D42683DD-2B26-11D7-8648000102C1865D

Henriksen, S., Hampson, G. J., Helland-Hansen, W., Johannessen, E. P., & Steel, R. J. (2009). Shelf edge and shoreline trajectories, a dynamic approach to stratigraphic analysis. *Basin Research*, *21*(5), 445–453. https://doi.org/10.1111/j.1365-2117.2009.00432.x

Ings, S. J., & Beaumont, C. (2010). Shortening viscous pressure ridges, a solution to the enigma of initiating salt 'withdrawal' minibasins. *Geology*, *38*(4), 339–342. https://doi.org/10.1130/G30520.1

Jenkins, C. (2018). Sediment accumulation rates for the Mississippi delta region: A time-interval synthesis. *Journal of Sedimentary Research*, *88*(2), 301–309. https://doi.org/10.2110/jsr.2018.15

Jia, H., Ji, H., & Yu, J. (2021). Shoreline trajectory and stratal stacking patterns: Relation to sediment partitioning and types of deep-lacustrine deposits. *Journal of Petroleum Science and Engineering*, *203*, 108537. https://doi.org/10.1016/j.petrol.2021.108537

Jordan, T. E., & Flemings, P. B. (1991). Large-scale stratigraphic architecture, eustatic variation, and unsteady tectonism: A theoretical evaluation. *Journal of Geophysical Research*, *96*(B4), 6681–6699. https://doi.org/10.1029/90JB01399

Karlo, J. F., van Buchem, F. S., Moen, J., & Milroy, K. (2014). Triassic-age salt tectonics of the central North Sea. *Interpretation*, *2*(4), SM19–SM28. https://doi.org/10.1190/INT-2014-0032.1

Kim, W., Paola, C., Voller, V. R., & Swenson, J. B. (2006). Experimental measurement of the relative importance of controls on shoreline migration. *Journal of Sedimentary Research*, *76*(2), 270–283. https://doi.org/10.2110/jsr.2006.019

Kopp, R. E., Simons, F. J., Mitrovica, J. X., Maloof, A. C., & Oppenheimer, M. (2009). Probabilistic assessment of sea level during the last interglacial stage. *Nature*, *462*(7275), 863–867. https://doi.org/10.1038/nature08686

Liesa, C. L., Soria, A. R., Meléndez, N., & Meléndez, A. (2006). Extensional fault control on the sedimentation patterns in a continental rift basin: El Castellar Formation, Galve sub-basin, Spain. *Journal of the Geological Society*, *163*(3), 487–498. https://doi.org/10.1144/0016-764904-169

Loncke, L., Gaullier, V., Mascle, J., Vendeville, B., & Camera, L. (2006). The Nile deep-sea fan: An example of interacting sedimentation, salt tectonics, and inherited subsalt paleotopographic features. *Marine and Petroleum Geology*, *23*(3), 297–315. https://doi.org/10.1016/j.marpetgeo.2006.01.001

Mansour, J., Giordani, J., Moresi, L., Beucher, R., Kaluza, O., Velic, M., et al. (2020). Underworld2: Python geodynamics modelling for desktop, HPC and cloud (v2.10.0b) [Software]. *Zenodo*. https://doi.org/10.5281/zenodo.3975252

Mellere, D., Plink-Bjorklund, P., & Steel, R. (2002). Anatomy of shelf deltas at the edge of a prograding Eocene shelf margin, Spitsbergen. *Sedimentology*, *49*(6), 1181–1206. https://doi.org/10.1046/j.1365-3091.2002.00484.x

Mikeš, D., ten Veen, J. H., Postma, G., & Steel, R. (2015). Inferring autogenically induced depositional discontinuities from observations on experimental deltaic shoreline trajectories. *Terra Nova*, *27*(6), 442–448. https://doi.org/10.1111/ter.12178

Minelli, L., Billi, A., Faccenna, C., Gervasi, A., Guerra, I., Orecchio, B., & Speranza, G. (2013). Discovery of a gliding salt-detached megaslide, calabria, ionian sea, Italy. *Geophysical Research Letters*, *40*(16), 4220–4224. https://doi.org/10.1002/grl.50818

Moresi, L., Mühlhaus, H.-B., Lemiale, V., & May, D. (2007). Incompressible viscous formulations for deformation and yielding of the lithosphere. In G. D. Karner, G. Manatschal, & L. M. Pinheiro (Eds.), *Imaging, Mapping and Modelling Continental Lithosphere Extension and Breakup* (Vol. 282, pp. 457–472). Geological Society of London. https://doi.org/10.1144/SP282.19

Moresi, L. N., Dufour, F., & Muhlhaus, H. B. (2003). A Lagrangian integration point finite element method for large deformation modeling of viscoelastic geomaterials. *Journal of Computational Physics*, *184*(2), 476–497. https://doi.org/10.1016/S0021-9991(02)00031-1

Mourgues, R., Lecomte, E., Vendeville, B., & Raillard, S. (2009). An experimental investigation of gravity-driven shale tectonics in progradational delta. *Tectonophysics*, *474*(3–4), 643–656. https://doi.org/10.1016/j.tecto.2009.05.003

Muto, T. (2001). Shoreline autoretreat substantiated in flume experiments. *Journal of Sedimentary Research*, *71*(2), 246–254. https://doi.org/10.1306/091400710246

Muto, T., & Steel, R. J. (1992). Retreat of the front in a prograding delta. *Geology*, *20*(11), 967–970. https://doi.org/10.1130/0091-7613(1992)020<0967:ROTFIA>2.3.CO;2

Paoletti, V., Milano, M., Baniamerian, J., & Fedi, M. (2020). Magnetic field imaging of salt structures at Nordkapp basin, Barents Sea. *Geophysical Research Letters*, *47*(18), e2020GL089026. https://doi.org/10.1029/2020GL089026

Patruno, S., Hampson, G. J., Jackson, C. A.-L., & Whipp, P. S. (2015). Quantitative progradation dynamics and stratigraphic architecture of ancient shallow-marine clinoform sets: A new method and its application to the upper Jurassic Sognefjord formation, troll field, offshore Norway. *Basin Research*, *27*(4), 412–452. https://doi.org/10.1111/bre.12081

Patruno, S., & Helland-Hansen, W. (2018). Clinoforms and clinoform systems: Review and dynamic classification scheme for shorelines, subaqueous deltas, shelf edges and continental margins. *Earth-Science Reviews*, *185*, 202–233. https://doi.org/10.1016/j.earscirev.2018.05.016

Pichel, L. M., Huismans, R. S., Gawthorpe, R., & Faleide, J. I. (2024). Post-salt carbonates control salt-tectonic minibasin formation. *Geology*, *52*(1), 82–86. https://doi.org/10.1130/G51717.1

Pirmez, C., Pratson, L. F., & Steckler, M. S. (1998). Clinoform development by advection-diffusion of suspended sediment: Modeling and comparison to natural systems. *Journal of Geophysical Research*, *103*(B10), 24141–24157. https://doi.org/10.1029/98JB01516

Prather, B. E., O'Byrne, C., Pirmez, C., & Sylvester, Z. (2017). Sediment partitioning, continental slopes and base-of-slope systems. *Basin Research*, *29*(3), 394–416. https://doi.org/10.1111/bre.12190

Ritchie, B. D., Gawthorpe, R. L., & Hardy, S. (2004). Three-dimensional numerical modeling of deltaic depositional sequences 1: Influence of the rate and magnitude of sea-level change. *Journal of Sedimentary Research*, *74*(2), 203–220. https://doi.org/10.1306/091303740203

Rojo, L. A., Marín, D., Cardozo, N., Escalona, A., & Koyi, H. (2020). The influence of halokinesis on prograding clinoforms: Insights from the Tiddlybanken Basin, Norwegian Barents Sea. *Basin Research*, *32*(5), 979–1004. https://doi.org/10.1111/bre.12411

Rovere, A., Stocchi, P., & Vacchi, M. (2016). Eustatic and Relative Sea Level changes. *Current Climate Change Reports*, *2*(4), 221–231. https://doi.org/10.1007/s40641-016-0045-7

Rowan, M. G., Peel, F. J., & Vendeville, B. C. (2004). Gravity-driven fold belts on passive margins. In K. R. McClay (Eds.), *Thrust Tectonics and Hydrocarbon Systems*. https://doi.org/10.1306/M82813C9

Stathopoulou, A., Papatheodorou, G., Tripsanas, E. K., Ferrari, A., Rubi, R., Geraga, M., et al. (2025). Clinoform architecture influenced by salt tectonics and Quaternary Sea level changes: The Acheloos delta complex, Gulf of Patras, Greece. *Marine Geology*, *482*, 107494. https://doi.org/10.1016/j.margeo.2025.107494

Steckler, M. S., Mountain, G. S., Miller, K., Miller, K., & Christie-Blick, N. (1999). Reconstruction of Tertiary progradation and clinoform development on the New Jersey passive margin by 2-D backstripping. *Marine Geology*, *154*(1–4), 399–420. https://doi.org/10.1016/S0025-3227(98)00126-1

Steel, R., & Olsen, T. (2002). Clinoforms, clinoform trajectories and deepwater sands. In J. M. Armentrout & N. C. Rosen (Eds.), *SEPM society for sedimentary geology*, *Sequence stratigraphic models for exploration and production: Evolving methodology, emerging models and application histories* (Vol. 22, pp. 367–380). https://doi.org/10.5724/gcs.02.22

Steel, R., Osman, A., Rossi, V. M., Alabdullatif, J., Olariu, C., Peng, Y., & Rey, F. (2024). Subaqueous deltas in the stratigraphic record: Catching up with the marine geologists. *Earth-Science Reviews*, *256*, 104879. https://doi.org/10.1016/j.earscirev.2024.104879

Steel, R. J., Carvajal, C., Petter, A. L., & Uroza, C. (2008). Shelf and shelf-margin growth in scenarios of rising and falling Sea Level. In G. J. Hampson, R. J. Steel, P. M. Burgess, & R. W. Dalrymple (Eds.), *Recent advances in models of siliciclastic shallow-marine stratigraphy* (Vol. 90, pp. 47–71). *SEPM Society for Sedimentary Geology*. https://doi.org/10.2110/pec.08.90.0047

Swenson, J., VOLLER, V., PAOLA, C., Parker, G., & MARR, J. (2000). Fluvio-deltaic sedimentation: A generalized stefan problem. *European Journal of Applied Mathematics*, *11*(5), 433–452. https://doi.org/10.1017/S0956792500004198

Tomer, A., Muto, T., & Kim, W. (2011). Autogenic hiatus in fluviodeltaic successions: Geometrical modeling and physical experiments. *Journal of Sedimentary Research*, *81*(3), 207–217. https://doi.org/10.2110/jsr.2011.19

Vail, P. R., Mitchum, R., Jr., & Thompson, S., III. (1977). Seismic stratigraphy and global changes of Sea Level: Part 4. Global cycles of relative changes of Sea Level: Section 2. Application of seismic reflection configuration to stratigraphic interpretation. In C. E. Payton (Ed.), *Seismic stratigraphy - Applications to hydrocarbon exploration* (Vol. 26, pp. 83–97). *AAPG Memoir*. https://doi.org/10.1306/M26490C6

Vendeville, B. C. (2005). Salt tectonics driven by sediment progradation: Part I—Mechanics and kinematics. *AAPG Bulletin*, *89*(8), 1071–1079. https://doi.org/10.1306/03310503063

Vendeville, B. C., & Jackson, M. P. A. (1992). The rise of diapirs during thin-skinned extension. *Marine and Petroleum Geology*, *9*(4), 331–354. https://doi.org/10.1016/0264-8172(92)90047-I

Wang, J., & Muto, T. (2021). Autostratigraphic modelling of the growth of alluvial-shelf systems during steady base-level cycles: Two-dimensional tank experiments. *Sedimentology*, *68*(1), 135–167. https://doi.org/10.1111/sed.12789

Wang, J., Muto, T., & Hajime, N. (2020). The grade index model as a rationale for autogenic nonequilibrium responses of deltaic clinoform to relative sea-level rise. *Basin Research*, *32*(2), 378–387. https://doi.org/10.1111/bre.12418

Wang, R., Kim, W., Colombera, L., Mountney, N. P., Lee, Y., & Lee, J. (2024). Autogenic evolution of valley-confined deltas during sea-level rise: Insights from numerical and physical modelling. *Sedimentology*, *71*(5), 1389–1418. https://doi.org/10.1111/sed.13178

Zhang, J. B., Liu, Y. S., Foley, S. F., Moynier, F., Zhao, L., Xu, R., & Wang, C. Y. (2024). Widespread two-layered melt structure in the asthenosphere. *Nature Geoscience*, *17*(5), 472–477. https://doi.org/10.1038/s41561-024-01433-1